Heliyon 6 (2020) e05213

Contents lists available at ScienceDirect

Heliyon

journal homepage: www.cell.com/heliyon

Research article

Effects of high hydrostatic pressure processing on structure and functional properties of biodegradable film

Sheyla Moreira Gonçalves [a,*], Davy William Hidalgo Chávez [a], Léa Mariza de Oliveira [d], Claire Isabel Grígoli de Luca Sarantópoulos [d], Carlos Wanderley Piler de Carvalho [a,c], Nathália Ramos de Melo [a,b], Amauri Rosenthal [a,c]

[a] Department of Food Science and Technology, Rodovia 465 - Km 7, UFRRJ, Seropédica, RJ 23891-360, Brazil
[b] Department of Agribusiness Engineering, Av. dos Trabalhadores 420 - Vila Sta. Cecília, UFF, Volta Redonda, RJ 27255-125, Brazil
[c] Embrapa Food Technology, Av. das Américas, 29501, Guaratiba, Rio de Janeiro, RJ 23020-470, Brazil
[d] Packaging Technology Center Cetea, Food Technology Institute Ital, Campinas, São Paulo, Brazil

ARTICLE INFO

Keywords:
Materials science
Food science
Emerging technology
Cellulose acetate
Packaging materials
Heat seal strength
Physicochemical properties

ABSTRACT

Effects of high hydrostatic pressure (HHP) processing (200–400 MPa/5 or 10 min) on functional properties of cellulose acetate (CA) films were investigated. As for mechanical properties, HHP caused a reduction in tensile strength (TS), Young's modulus (YM) and an increase in elongation at break (EB). The pressurized films were more luminous, yellowish, reddish and opaque. Less affinity for water was detected for pressurized films through analyses of contact angle and moisture absorption, in addition to reducing the water vapor transmission rate (WVTR). Scanning electron microscopy (SEM) showed the occurrence of delamination for most films, except those treated with 200 MPa/10 min and 300 MPa/10 min. All films showed a predominance of amorphous structure in X-ray diffraction analysis (XRD). That is alignment with the results of differential scanning calorimetry (DSC), which presented values for glass transition temperature (Tg), water adsorption and melting temperature characteristic of materials with low crystallinity. Films treated with HHP had better mechanical resistance during the sealing at 250 °C. In overall the results confirmed the minimal influence of HHP on the functional properties of the CA film and contributed to the scientific and technological knowledge for its potential application in foods processed by HHP.

1. Introduction

Among the polymers used to make food packaging, non-biodegradable plastics derived from petroleum is the best-known and has the broadest use. However, in view of the growing global environmental awareness, natural polymers are gradually gaining industrial importance (Siracusa et al., 2008). Cellulose acetate (CA) is a biodegradable and abundant polymer, synthesized industrially through the acetylation of cellulose with acetic anhydride and acetic acid with sulfuric acid as a catalyst (Cerqueira et al., 2010). For the production of CA, the hydroxyl groups of the glycosidic bound units of the cellulose chain are replaced by acetyl groups, thus generating a cellulose ester. In this way, different types of CA can be elaborated according to the degree of substitution (number of acetyls linked to hydroxyls). CA has a specific weight of 1.32 g/cm-3 and decomposes at a temperature of 240 °C. Its properties vary according to the degree of acetylation, quantity and quality of additives used, but it is usually a rigid and compact material. It can be used in different applications such as in the production of transparent adhesive tape, tool handles, eyeglass frames, films with controlled release of active substances, textiles, composites and polymeric membranes. It is a thermoplastic material with good impact resistance, transparent and good water vapor barrier properties (Miles and Briston, 1975; Canevarolo, 2006).

For achieving specific functional properties CA films have been made with the addition of plasticizers (Gonçalves et al., 2019; Liu et al., 2019; Richardson et al., 2014) and antimicrobial compounds (Dannenberg et al., 2017; Gonçalves et al., 2019; Zizovic et al., 2018), thus fulfilling its potential for preparing packaging for direct contact with food. According to a literature study, polymers that have amorphous and crystalline segments have difficulty in segregation during film making, since the amorphous region has greater miscibility power when compared to the crystalline region, favoring greater resistance to traction (Rana et al.,

* Corresponding author.
E-mail address: sheylapa1@hotmail.com (S.M. Gonçalves).

https://doi.org/10.1016/j.heliyon.2020.e05213
Received 4 June 2020; Received in revised form 5 August 2020; Accepted 7 October 2020

1999, 2000). In addition, the morphology of the polymer chains directly reflect the compatibility between the polymer matrix and the incorporated compounds (Song et al., 2020), with a consequent influence on the mechanical and thermal properties (Hasa et al., 2020). However, according to Gonçalves et al. (2019) CA film is predominantly amorphous, which suggests less segregation between the chains, greater miscibility power and greater uniformity of mechanical properties.

High hydrostatic pressure (HHP) is a non-thermal technology that is increasingly used by the food industry in order to meet the desires of consumers who demand safe, nutritious and closer to natural foods. It is a process where the food is subjected to a certain pressure distributed evenly to the product for a set time, which ensures that the food maintains its initial shape even in the face of extreme pressures (Oliveira et al., 2015; Stratakos et al., 2015). The packaging used to pack the food to be pressurized must have the capacity to withstand the change in volume since during the pressure increase the volume of the food reduces and, soon after, expands during decompression (Fellows, 2006). In addition, during volume reduction high pressure can favor chemical reactions and changes in molecular and structural conformation of the organic and inorganic polymeric matrixes (Galazka et al., 2000; Gross and Jaenicke, 1994). Such characteristics justify the widespread use of HHP for structural modification of proteins, enzymes or polysaccharides (Fellows, 2006; Molinaro et al., 2015). Studies on the effects of HHP on synthetic polymeric films have shown both reversible and irreversible changes. In response to high pressure conditions, changes in the crystalline and amorphous phases can occur, which directly reflects on the functional properties of polymeric packaging (Mensitieri et al., 2013). Therefore, it is of fundamental importance to predict the possible effects caused by HHP on the properties of the packaging, since extreme changes in the structure can make its application impossible (Fraldi et al., 2014).

According to Martins (2014), there was a notable lack of studies on the possible changes caused by HHP on the structures and functional properties of biodegradable polymers, which it is still verified in the literature. Furthermore, no study has investigated the effect of HHP on functional properties of CA films according to our knowledge. Therefore, this study aimed to submit a CA film to HHP processing at different pressure and time levels and evaluate the structural and functional changes in the film. The films were characterized in terms of visual appearance, barrier properties (water vapor), thermal properties (DSC), mechanical properties, heat sealing, contact angle, moisture absorption, chemical interactions based on FTIR and DRX analyses and morphological changes by SEM.

2. Materials and methods

2.1. Materials

Cellulose acetate (CA) and Acetone (p.a.) was purchased from Sigma-Aldrich, Brazil.

2.2. Preparation of films and application of HHP

By means of the casting method (Melo, 2003), the gels formed by the solubilization of CA in acetone (1:10 w/v) were poured into a glass plate, spread with the aid of a glass stick and dried under controlled conditions (temperature of 25 ± 2 °C and 75% humidity) for 10 min. After drying, the films were detached from the plates, packed in a vacuum in sterile bags with identification stripe (Nasco Whirl-Pak) and subjected to HHP processing (200, 300 or 400 MPa for 5 or 10 min) in Stansted Fluid Power, model S-FL-850-9-W. The films were preconditioned at 75% relative humidity, for a maximum of 5 days, to carry out the analyses. The control film was made without HHP.

2.3. Visual aspects

Samples of 4 × 4 cm were evaluated using the Minolta CM-5-ID colorimeter for the degree of brightness L*, red/green chromaticity (±a*), yellow/blue chromaticity (±b*), total difference (ΔE*), Chroma (intensity or saturation of color (C*)) and Opacity (Romani et al., 2017). Hue angle (h^o) locates the color in polar coordinates and is expressed in degrees: 0° for red (+a*), 90° for yellow (+b*), 180° for green (-a*), and 270° for blue (-b*).

2.4. Mechanical analyses

The TA.XTplus texturometer (Stable Micro Systems, Surrey, England), operating according to ASTM standard method D 882-82, was used to determine tensile strength (TS) (MPa), elongation at break (EB) (%) and Young's modulus (YM) (MPa). Specimens of 5 × 2 cm films were fixed in a texturometer with initial separation of 25 mm, operated with a 30 kg cell, with a force of 0.049 N and a velocity of 1 mm/s. With the help of Exponent Texture TEE32 (Stable Micro Systems), the TS was obtained through the relation of the maximum force (N) by the sample area (mm). The YM was calculated from the linear region of the stress versus strain curve. The EB was calculated according to Eq. (1).

$$EB = \frac{L}{C_i} \times 100 \quad (1)$$

In which,
EB: elongation at rupture expressed in %;
L: Deformation expressed in mm;
Ci: Initial sample length in mm.

2.5. Contact angle

The wettability of the films was obtained using a contact angle meter (model CAM 101, KSV Instruments, Finland), equipped with diffuse light, DMK 21AF04 camera (1 photo/s) and syringe with distilled water (Nascimento et al., 2012). Three drops of distilled water (2 μl) were deposited on the surface of each film (20 mm long and 10 mm wide), fixed on a glass slide using double-sided tape. The image of each drop was taken by digital camera at 1s intervals for 30 s. The contact angle was calculated from the average of the right and left angles of the drop, as a function of the analysis time (30 s).

2.6. Moisture absorption

Samples of 20 mm × 20 mm were oven dried at 100 °C/2 h, maintained at 0 % relative humidity (RH) for 24 h and then weighed. Then, the samples were conditioned in a desiccator containing saturated NaCl solution with 75% RH for 7 days, and the final weighing was performed (Alizadeh-Sania et al., 2018). RH was calculated according to Eq. (2).

$$MA = \frac{W_t - W_0}{W_0} \times 100 \quad (2)$$

Where,
MA: relative humidity in %;
W_0: initial weight;
W_t: final weight after 7 days.

2.7. Water vapor transmission rate (WVTR)

Water vapor transmission rate (WVTR) was determined gravimetrically, according to the (ASTM E96-95) with modifications, under a relative humidity gradient of 75%. The tests were conducted in triplicate.

2.8. Fourier transform infrared attenuated total reflection (FTIR-ATR) spectroscopy

The changes in the chemical structure of CA films as a result of the action of HHP were characterized using Perkin Elmer (Spectrum 100) under attenuated total reflection (ATR) mode. The spectrum was recorded in the wavelength range of 650–4000 cm^{-1}, 4 cm^{-1} resolution and 32 scans.

2.9. Scanning electron microscopy (SEM)

Images of the surfaces and fracture regions of the films were obtained with the help of the Scanning Electron Microscope (Carl Zeiss, model EVO MA 10). Specimens of 1 × 0.5 cm were fixed in "stub", covered with gold (Au) (metallizer EMITEC K550X) with current of 25 mA/2 min and observed in the SEM in low vacuum, using an acceleration voltage of 5000 kV, 450 of filament current, and scans of 5000 and 500x.

2.10. X-ray diffraction (XRD)

XRD curves were obtained using a Phaser D2 Bruker Diffractometer (Bruker, Germany), operated at 30 kV and 10 mA. After conditioning at 75% relative humidity, two specimens of each film with 2 cm of diameter were fixed in specific support and analyzed in the range of 2 to 29° and ω-2θ (Candido et al., 2017).

2.11. Differential scanning calorimetry (DSC)

DSC thermograms were obtained using a Q200 DSC (TA Instruments, New Castle, USA). All films were preconditioned to 75% relative humidity for 48 h. Then, 3.5 mg samples were sealed in aluminum capsules and heated to 20–250 °C at a rate of 10 °C/min and cooled at a rate of 20 °C/min. The glass transition temperature (Tg) was determined by a second heating curve of 20–250 °C with a heating rate of 10 °C/min.

2.12. Heat sealing tensile strength

The sealing curves were determined according to the ASTM F 2029-08 standard in two stages: heat sealing of the specimens and determination of the tensile strength of the heat sealing. The heat seals of the specimens were made in a Brugger heat sealer operating with two heated jaws with a smooth profile and 5 mm wide with Teflon coating operating with a force of 300 N (pressure = 4 bar) and contact time of 1 s. The temperatures of the two sealing jaws were set in the range of 240 °C–260 °C. The specimens were prepared in a controlled temperature environment (23 °C) after conditioning the samples in an environment at 23 °C ± 2 °C and 50 ± 5% relative humidity for at least 48 h. The resistance of the heat seal to traction until the occurrence of failure was determined according to the ASTM F 88/F 88M-09 standard. Specimens 25.4 mm wide were inserted in an Instron universal testing machine model 5966-E2 operating with a 100 N load cell at a speed of 300 mm/min. The distance between the fixing claws was 25 mm. The test was carried out in at 23 °C ± 2 °C and 50 ± 5% relative humidity after conditioning the specimens in that same environment for at least 24 h.

2.13. Statistical analyses

Statistical analyses were performed using software R, version 3.2.4 (R Foundation for Computational Statistics, Vienna, Austria) and FactoMineR version 1.32. The Tukey multi comparative test was used to obtain differences between samples after ANOVA test both (Tukey and ANOVA tests) with a significance level of 5%. In addition, possible correlations between treatments and/or variables were investigated with the help of Pearson's Correlation. The stronges of Pearson's correlation was evaluated following the rule proposed by Teles et al. (2019).

3. Results and discussion

3.1. Visual aspects

According to Table 1, HHP increased Luminosity (L*) and total difference (ΔE*). HHP processing resulted in films with lower color saturation (C*) and less intense red (+a*) and yellow (+b*) colors, as compared to the control film (CAP0T0). For hue angle (h^o), the color of all films was between 0° (red) and 90° (yellow), but HHP caused an increase in the mean values for the CAP200T10 film and reduction of the values for the CAP400T5 and CAP400T10 films.

HHP treatments caused an increase in the opacity of all films, being the film CAP400T10 the most opaque. This effect may be justified by the possible closure of spaces in the polymeric chemical structure due to the applied pressure (Yoo et al., 2013) preventing passage of light beams through the sample. Most treatments lasting 10 min caused a slight increase in L*, ΔE*, opacity, and reduction of b*, C*, and h^o, when compared to 5 min processes.

3.2. Mechanical analysis

The mechanical properties of the CA film were influenced by both the pressure and the time of the process (Table 2). A reduction of tensile strength (TS) and Young's modulus (YM) was observed for all HHP conditions, especially the film with 300 MPa/5 min (CAP300T5), which presented the least resistance and rigidity. Structural changes in polymeric films can occur in different HHP conditions, which can be reflected in the mechanical functions of the packaging. Such effect may happen due to changes in crystallinity, film delamination, or plastification caused by HHP (Marangoni Júnior et al., 2019). Therefore, the results reveal that the HHP conditions may have caused modifications in the chemical structure of the CA film, leading to a certain fragility to the material.

The increase in elongation at break (EB) of the films treated with HHP (Table 2) are in agreement with the other mechanical properties, and the highest EB was presented by the film with lower TS (CAP300T5). TS and EB are usually the mechanical parameters most used to characterize food packaging (Khaneghah et al., 2018).

3.3. Contact angle, moisture absorption (MA) and water vapor transmission rate (WVTR)

According to Table 2, only the CAP200T10 and CAP300T10 films did not differ from the control film (CAP0T0) for the contact angle. The other HHP conditions presented an increase in the contact angle, indicating a lower affinity of the films surface for the water and, consequently, a lower degree of wettability. The HHP conditions may have caused changes in the intermolecular forces of the CA film (CAHHP) in such a way that the balance of these forces was greater than the forces of interaction between water and surface of the films. When the surface tension is greater than the attraction force of water to the film surface, the contact will be restricted and so that the droplet will become more spherical with greater contact angle. In this sense, when deposited on the surface of the film, the water droplet contracted, forming a more spherical droplet (Sarafraz and Arjomandi, 2019).

The results in Table 2 show that the highest values for moisture absorption (MA) were observed for the films that presented the lowest values for contact angle (CAP0T0, CAP200T10 and CAP300T10). On the contrary, in the same way the films with the lowest MA capacity were those with higher contact angle CAP300T5, CAP400T5 and CAP400T10. Therefore, the lower affinity for water by the film surfaces, caused by the HHP conditions, may have prevented the water molecules from being absorbed in the polymer matrix. The CAP200T5 film despite having a higher contact angle showed a higher moisture absorption capacity. This phenomenon may be associated to the greater delamination inside the film which, in turn, may have allowed the passage of water through the spaces in the polymer matrix.

Table 1. Visual appearance of the cellulose acetate films treated with high hydrostatic pressure (200, 300 or 400 MPa/5 or 10 min) in comparison to non-pressurized control.

Samples	L*	a*	b*	ΔE*	C*	h°	Opacity
CA P0T0	97.13 ± 0.2^{b}	0.04 ± 0.01^{a}	0.32 ± 0.07^{a}	2.88 ± 0.18^{c}	0.33 ± 0.06^{a}	82.83 ± 1.6^{b}	92.81 ± 0.49^{b}
CA P200T5	97.20 ± 0.02^{ab}	0.01 ± 0.01^{c}	0.17 ± 0.01^{b}	3.35 ± 0.05^{b}	0.16 ± 0.01^{b}	85.85 ± 0.99^{a}	92.97 ± 0.05^{ab}
CA P200T10	97.24 ± 0.02^{ab}	0.02 ± 0^{b}	0.14 ± 0.01^{bc}	3.4 ± 0.03^{ab}	0.14 ± 0.01^{bc}	82.65 ± 0.52^{b}	93.06 ± 0.04^{ab}
CA P300T5	97.22 ± 0.02^{ab}	0.02 ± 0^{b}	0.14 ± 0.01^{bc}	3.42 ± 0.05^{ab}	0.14 ± 0.01^{bc}	81.89 ± 1.04^{b}	93.02 ± 0.05^{ab}
CA P300T10	97.22 ± 0.05^{ab}	0.02 ± 0^{b}	0.12 ± 0.01^{c}	3.5 ± 0.05^{a}	0.12 ± 0.01^{c}	81.61 ± 0.81^{b}	93.01 ± 0.11^{ab}
CA P400T5	97.24 ± 0.02^{ab}	0.02 ± 0^{b}	0.12 ± 0.01^{c}	3.48 ± 0.03^{a}	0.12 ± 0.01^{c}	79.76 ± 1.38^{c}	93.06 ± 0.05^{ab}
CA P400T10	97.25 ± 0^{a}	0.02 ± 0^{b}	0.11 ± 0.01^{c}	3.50 ± 0.03^{a}	0.11 ± 0.01^{c}	79.65 ± 1.21^{c}	93.09 ± 0.01^{a}

P: Pressure level (MPa) and T: Treatment time (min.); CAP0T0: control film without high pressure treatment; *Mean values followed by the same letters in the same column do not differ ($p > 0.05$) by the Tukey test at the 5% level of significance. The results are expressed as mean ($n = 4$) ± standard deviation.

Table 2. Mechanical properties, contact angle, and moisture absorption of cellulose acetate films treated with high hydrostatic pressure (200, 300 and 400 MPa/5 and 10 min) in comparison to non-pressurized control.

Samples	TS (MPa)	YM (Mpa)	EB (%)	Contact angle (°)	Moisture absorption (%)	WVTR (g.m^{-2}. day^{-1})
CAP0T0	40.9 ± 1.2^{a}	1894.9 ± 31.5^{a}	4.2 ± 0.1^{c}	57.46 ± 1.4^{c}	0.06 ± 0.0^{ab}	232.56 ± 2.29^{a}
CAP200T5	34.5 ± 1.5^{bcd}	1342.1 ± 69.1^{b}	5.5 ± 0.3^{b}	61.65 ± 0.2^{b}	0.05 ± 0.0^{abc}	205.57 ± 4.48^{b}
CAP200T10	34.9 ± 1.1^{bc}	1347.1 ± 58.4^{b}	5.5 ± 0.3^{b}	58.61 ± 0.3^{c}	0.05 ± 0.0^{abc}	197.84 ± 1.86^{c}
CAP300T5	28.9 ± 1.3^{e}	1104.4 ± 155.8^{c}	6.3 ± 0.4^{a}	65.85 ± 0.6^{a}	0.03 ± 0.0^{c}	192.35 ± 1.13^{d}
CAP300T10	36.6 ± 1.3^{b}	1483.1 ± 92.4^{b}	5.3 ± 0.3^{b}	58.23 ± 1.8^{c}	0.07 ± 0.0^{a}	185.78 ± 1.77^{e}
CAP400T5	32.4 ± 0.7^{d}	1131.3 ± 66.5^{c}	6.2 ± 0.3^{a}	59.68 ± 0.7^{bc}	0.04 ± 0.0^{c}	182.53 ± 0.68^{ef}
CAP400T10	32.6 ± 1.4^{cd}	1189.3 ± 37.1^{c}	5.8 ± 0.3^{ab}	65.76 ± 1.4^{a}	0.04 ± 0.0^{bc}	177.36 ± 2.26^{f}

P: Pressure level (MPa) and T: Treatment time (min.); CAP0T0: control film without high pressure treatment; *Mean values followed by the same letters in the same column do not differ ($p > 0.05$) by the Tukey test at the 5% level of significance. The results are expressed as mean ($n = 4$) ± standard deviation.

The treatment with HHP caused a reduction in the WVTR of all films (Table 2), which is in agreement with the results for the analysis of contact angle and moisture absorption, thus demonstrating a reduction in the affinity of the films for water. Molinaro et al. (2015) reported a reduction in WVTR in gelatin films treated with HHP (600 MPa/30 min) and attributed the results to a possible change in the stability of hydrogen bonds. The authors suggested that the greater structural compactness generated by HHP may explain the reduction in the passage of water molecules through the polymeric network.

3.4. Fourier transform infrared attenuated total reflection (FTIR-ATR) spectroscopy

FTIR spectra (Figure 1) show that the treatment of films with HHP did not cause detectable changes in their chemical structures. For CA production, cellulose-free hydroxyl groups are replaced by acetyl groups through the cellulose esterification process with acetic anhydride. The presence of a band at 1736 cm^{-1}, which may be associated with vibration of C=O in carboxylic acid, is characteristic of acetyl groups. According to

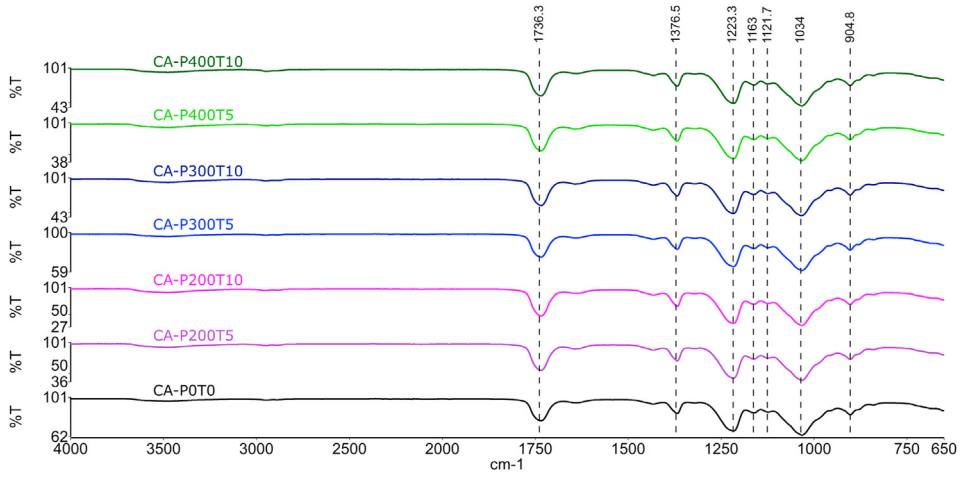

Figure 1. FTIR spectra of the cellulose acetate film (CAP0T0) and cellulose acetate films treated with high hydrostatic pressure (CAP200T5, CAP200T10, CAP300T5, CAP300T10, CAP400T5 and CAP400T10), in which P indicates pressure (MPa) and T is the time (min).

Liu et al. (2019), the presence of this peak indicates cellulose acetylation. The 1376 cm^{-1} band can be associated with vibration of the C–H bond, which in turn can also characterize bands of acetyl groups. In addition to these, the presence of bands at 1223, 1163, 1121 and 1034 cm^{-1} may be associated with the vibration of the ester group (C–O–C) of the acetate (Liu et al., 2019).

3.5. Scanning electron microscopy (SEM)

SEM images (Figure 2) for the surfaces of all CA films, treated or not with HHP, were homogeneous and smooth. Therefore, it is noted that all HHP processing conditions did not cause changes in the surface of the CA films. The fracture region of the film without HHP treatment (CA-P0T0 500 and 5000 x) also proved to be smooth and uniform. However, most of the CA films resulting from HHP treatment presented delamination in the fracture region, except for the CAP200T10 and CAP300T10 films, which was more homogeneous. Therefore, the lower means for TS (Table 2) presented by CA films processed by HHP may be associated with changes in their fracture regions. However, among the pressurized films the CAP200T10 and CAP300T10 films presented the highest TS (Table 2), which, in turn, can be justified by the apparent delamination within the free fracture region (Marangoni Júnior et al., 2019).

3.6. X-ray diffraction (XRD)

The Diffractograms revealed low crystallinity for all CA films (Figure 3), caused by cellulose acetylation. Small peaks can be observed in the region of $2\theta = 8.7^{\circ}$ and 23°. Crystalline diffraction of the CA

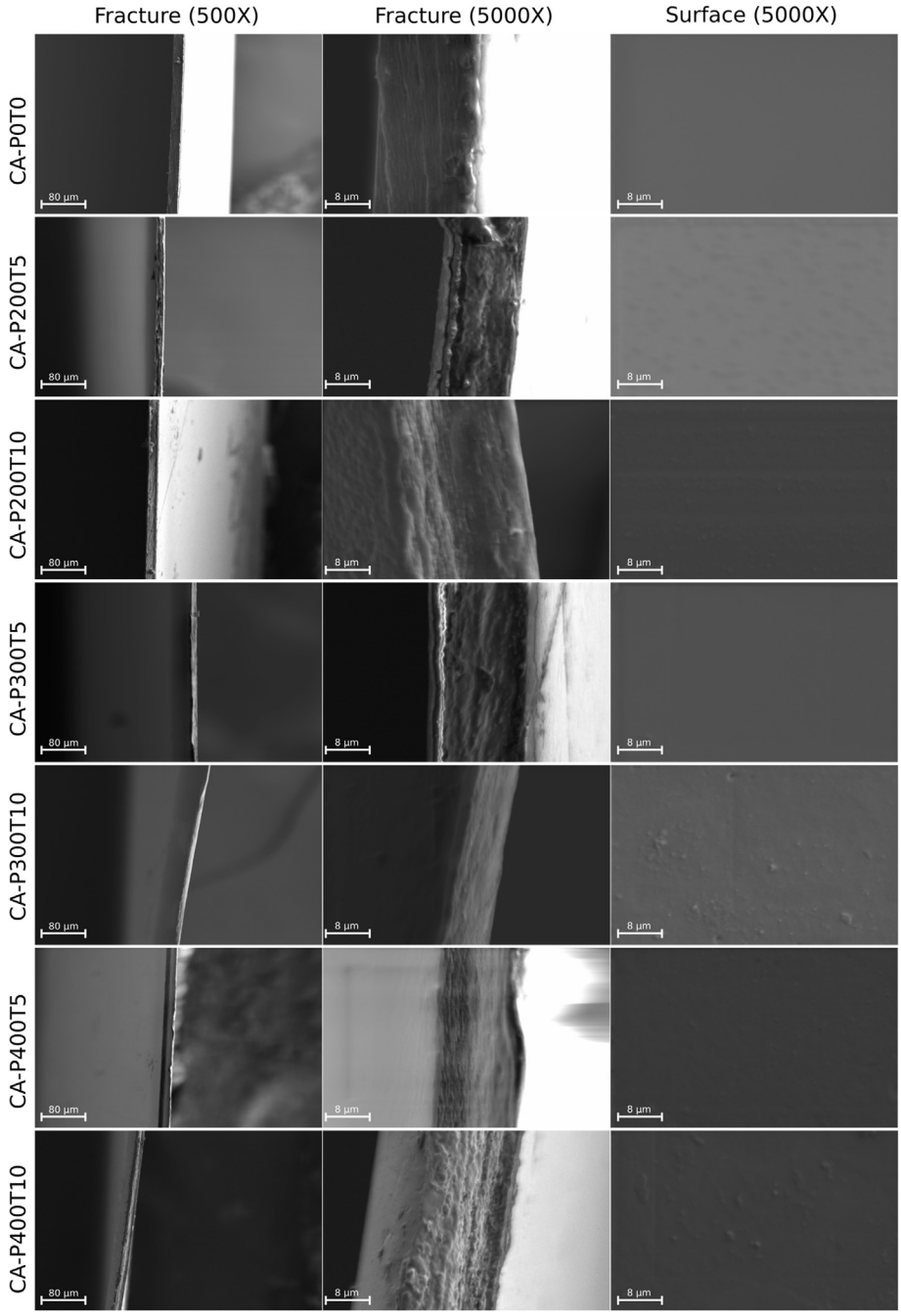

Figure 2. SEM of the surface and fracture region of the cellulose acetate film (CAP0T0) and cellulose acetate films treated with high hydrostatic pressure (CAP200T5, CAP200T10, CAP300T5, CAP300T10, CAP400T5 and CAP400T10), in which P indicates pressure (MPa) and T is the time (min).

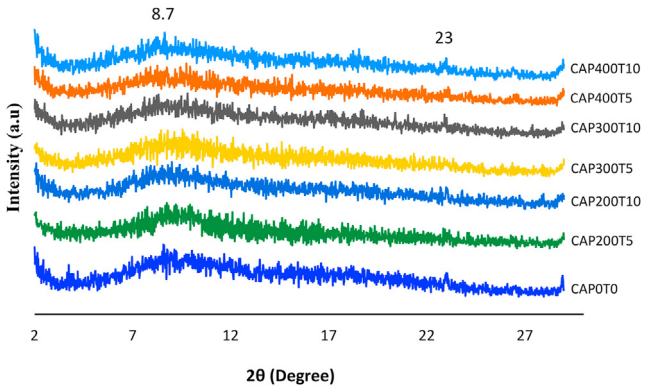

Figure 3. DRX Diffractograms of the CA film (CA-P0T0) and CA films treated with high hydrostatic pressure (CAP200T5, CAP200T10, CAP300T5, CAP300T10, CAP400T5, CAP400T10) (A), in which P indicates pressure (MPa) and T is the time (min).

usually occurs around $2\theta = 8$, 10, and 13° (Chen et al., 2016). Peaks in the region $2\theta = 8$ ° of CA are associated with the presence of the acetyl group in the cellulose chain, which, in turn, cause rupture in the cellulose fibrillar microstructure during the acetylation process (Wan Daud and Djuned, 2015). In this study, Figure 3 shows that the changes caused by HHP in the crystalline structure of the CA film were minimal being verified mainly in the region $2\theta = 8.7°$, resulting in slight reduction for the treatments at 300 MPa and 400 MPa. Furthermore, peak $2\theta = 23°$ showed a slight reduction only for CAP300T5 and CAP400T5. Castañón-Rodríguez et al. (2013) processed sugarcane bagasse with HPP and verified the presence of a characteristic cellulose peak between 22 and 23°. The authors reported that the XRD standards of the samples treated with HHP indicated modification of cellulose crystalline structure. However, the study suggested that the cellulose amorphous region may be more susceptible to treatment with HHP when compared to the crystalline region.

3.7. Differential scanning calorimetry (DSC)

Figure 4 shows changes caused by HHP on CA films regarding water adsorption capacity, glass transition temperature (Tg) and melting temperature. The endothermic peaks (EP) of the first curves correspond to water desorption events (Kendouli et al., 2014). The first endothermic peaks occurred between 100 and 150 °C and their variation depended on the moisture retention capacity of each film. According to the degree of substitution (DS) of CA these peaks can occur at different temperatures (de Freitas et al., 2017). However, although all films had the same DS, treatment with HHP caused a slight increase in the temperature of the second endothermic peaks of all films, except for CAP200T5, as shown in Figure 4.

The results for DSC (Figure 4) showed that Tg (first endothermic peak in second heating curve) of control CA film was 203 °C (I) (CAP0T0). Previous study showed that Tg of CA with a substitution degree of 1.48° located at around 223 °C (de Freitas et al., 2017). When submitted to the different HHP conditions CA films had a slight reduction in Tg ranging from 197.26 to 195.33 °C (I). The second peaks of the second heating curve represent the melting temperature of the films. The processing with HPP caused minimal changes in the melting temperature values, presenting temperatures in a narrow range between 227.66 (CAP400T10) to 226.59 °C (CAP200T10). XRD results obtained for Tg and melting temperature for CA films are in agreement with thermal properties of low crystallinity polymeric materials (Kendouli et al., 2014; de Freitas et al., 2017).

3.8. Heat sealing tensile strength

Resistance to mechanical stress during normal or adverse conditions is of fundamental importance to direct the application of packaging (Marangoni Júnior et al., 2020a). Therefore, thermal sealability and resistance to mechanical stress during heat sealing have been studied for different types of films (Hernandez-Lzquierdo and Krochta, 2009; Cho et al., 2010; Marangoni Júnior et al., 2020b). According to Figure 5 the sealing was restricted to the temperature range evaluated since it did not

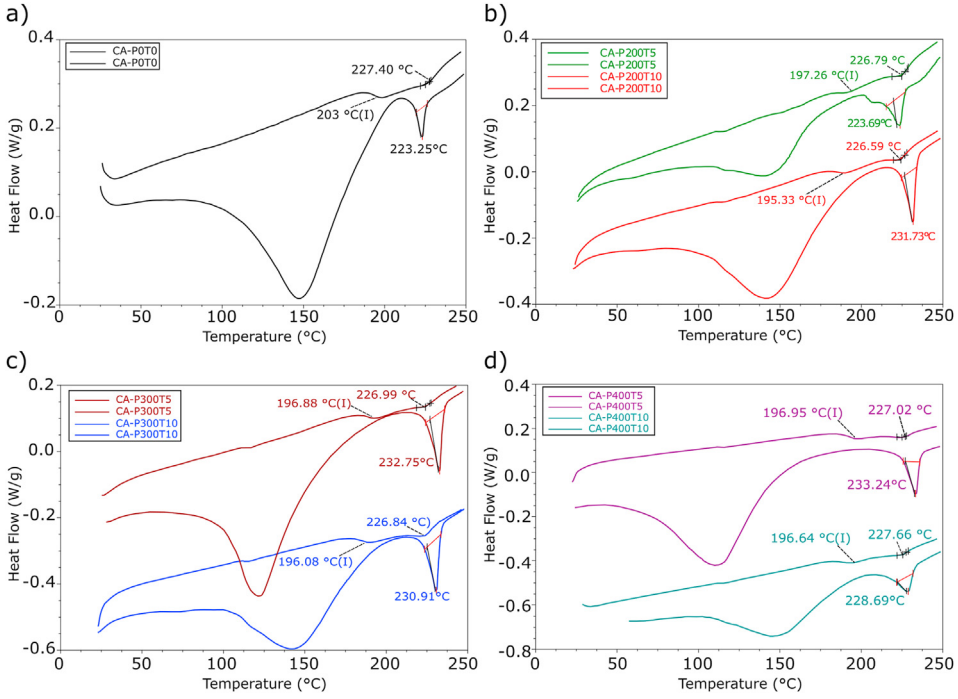

Figure 4. DSC thermograms of the CA film (a: CAP0T0) and CA films with HHP treatment (b: CAP200T5, CAP200T10; c: CAP300T5, CAP300T10; d: CAP400T5, CAP400T10), in which P indicates pressure (MPa) and T is the time (min).

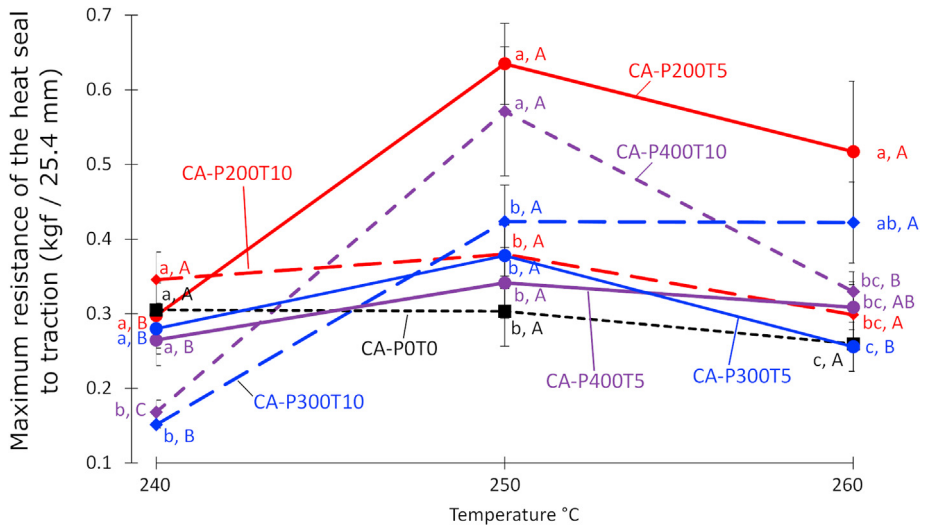

Figure 5. Sealing curves of the CA film (CAP0T0) and CA films with HHP treatment (CAP200T5, CAP200T10, CAP300T5, CAP300T10, CAP400T5 and CAP400T10), in which P indicates pressure (MPa) and T is the time (min).

occur at 230 °C but instead melted at 270 °C. Therefore, the sealing of all films came out at 240, 250 and 260 °C. For the films treated with HHP the highest seal strength was verified at 250 °C (Figure 5), thus achieving the highest means of 0.635 and 0.571 Kgf/25.4 mm for CA-P200T5 and CA-P400T10, respectively. The control film (CAP0T0) showed the highest seal strength at 240 °C followed by a slight reduction at higher temperatures.

CA-P300T10 and CA-P400T10 films presented the lowest resistances and statistical differences for sealing at 240 °C comparing to the film without high pressure processing (CA-P0T0). Concerning sealing at 260 °C, CA-P0T0 and CA-P300T5 films resulted in the lowest values for seal strength, while CA-P200T5 conditions provided the highest film seal strength at that temperature and the greatest resistant for sealing both at 250 and 260 °C. In addition, such film also presented the third highest seal resistance at 240 °C, suggesting in overall positively influence of 200 MPa/5 min processing to improve film heat sealing resistance. According to the data presented for XRD and DSC, all films were notably amorphous. Therefore, it is believed that the greater susceptibility of the amorphous domains to compression and decompression during HHP treatment (Castañón-Rodríguez et al., 2013) favored changes in the structure of the CA film, thus positively influencing the resistance of most films to sealing at 250 and 260 °C.

3.9. Pearson's correlation

In Table 3, strong or very strong positive correlations (Teles et al., 2019) occurred when the variables showed similar behavior in the face of the same HHP conditions (positive values highlighted in bold). Positive correlation was observed in: ΔE * with L *; b * with a *; C * with a * and b *; Opacity with L * and ΔE *; YM with b *, C * and TS; EB with L *, ΔE * and opacity; MA with TS and YM; WVTR with b *, C * and YM. In addition to these, strong or very strong negative correlations (negative values highlighted in bold) were observed b * with L *; ΔE * with a * and b *; C * with L * and ΔE *; Opacity with b * and C *; YM with L *, ΔE * and opacity; EB with b *, C *, TS and YM; Contact angle with TS; MA with contact angle; WVTR with L *, ΔE *, opacity and EB. In the negative

Table 3. Pearson's correlation for dependent variables for cellulose acetate films treated with high hydrostatic pressure.

Variables	L*	a*	b*	ΔE*	C*	h°	Opacity	TS	YM	EB	Contact angle	MA	WVTR	MRHST 240
a*	-0.701													
b*	**-0.965**	**0.784**												
ΔE*	**0.947**	**-0.803**	**-0.998**											
C*	**-0.958**	**0.820**	**0.998**	**-0.998**										
h°	-0.490	-0.196	0.414	-0.386	0.364									
Opacity	**0.999**	-0.697	**-0.961**	**0.941**	**-0.953**	-0.495								
TS	-0.730	0.635	0.740	-0.730	0.743	0.306	-0.746							
YM	**-0.866**	0.740	**0.862**	**-0.851**	**0.866**	0.365	**-0.876**	**0.958**						
EB	**0.828**	-0.700	**-0.842**	**0.835**	**-0.844**	-0.381	**0.836**	**-0.965**	**-0.989**					
Contact angle	0.436	-0.409	-0.442	0.433	-0.447	-0.218	0.469	**-0.792**	-0.687	0.645				
MA	-0.443	0.295	0.355	-0.326	0.355	0.288	-0.472	**0.847**	**0.765**	-0.754	**-0.781**			
WVTR	**-0.936**	0.630	**0.961**	**-0.956**	**0.948**	0.624	**-0.935**	0.709	**0.829**	**-0.813**	-0.479	0.372		
MRHST 240	-0.328	0.136	0.447	-0.471	0.429	0.529	-0.325	0.089	0.154	-0.146	-0.251	-0.218	0.601	
MRHST 250	0.295	-0.694	-0.359	0.381	-0.401	0.338	0.305	-0.228	-0.307	0.201	0.483	-0.086	-0.287	-0.296
MRHST 260	0.086	-0.660	-0.241	0.290	-0.288	0.548	0.071	0.093	-0.032	-0.012	-0.072	0.384	-0.117	-0.247

*Values in bold are different from 0 with a significance level alpha = 0.05.

correlations, the same HHP condition was able to cause opposite responses in the different variables. Table 3 also shows that the variables h° and heat sealing tensile strength (MRHST) did not show a strong correlation for either positive or negative. Therefore, it is concluded that the different HHP conditions caused changes in AC films for the studied variables.

4. Conclusions

Processing by HHP resulted in more luminous and opaque CA films, with lower color saturation and less intensity of red and yellow colors. In addition to these characteristics, HHP caused reduction of TS, YM, Tg, MA, WVTR besides increase of EB and contact angle. Fracture regions observed by SEM showed that most HHP treatment conditions evaluated caused delamination or slight porosity of CA films. Improvement in resistance to mechanical stress during heat sealing (250 °C) was shown by all pressurized films. Therefore, this study brought a promising approach on the use of AC films to pack food to be pressurized, without impairing its functional properties.

Declarations

Author contribution statement

Sheyla Moreira Gonçalves: Conceived and designed the experiments; Performed the experiments; Analyzed and interpreted the data; Wrote the paper.

Davy William Hidalgo Chávez: Analyzed and interpreted the data.

Léa Mariza de Oliveira, Claire Isabel Grígoli de Luca Sarantópoulos: Performed the experiments.

Carlos Wanderley Piler de Carvalhoa: Contributed reagents, materials, analysis tools or data.

Amauri Rosenthal, Nathália Ramos de Melo: Conceived and designed the experiments; Contributed reagents, materials, analysis tools or data; Wrote the paper.

Funding statement

This work was supported by Coordination of Improvement of Higher Education Personnel - Brazil (CAPES) (Financial Code 001), and Brazilian Agricultural Research Corporation - Brazil (Embrapa), and Carlos Chagas Filho Foundation for Research Support of the State of Rio de Janeiro - Brazil (FAPERJ).

Competing interest statement

The authors declare no conflict of interest.

Additional information

No additional information is available for this paper.

Acknowledgements

The authors express their sincere appreciation to the infrastructure including laboratory and pilot plant facilities were provided by Embrapa; LMME laboratory Federal Fluminense University-Volta Redonda-RJ; Federal Rural University of Rio de Janeiro (UFRRJ); and the Federal University of Fluminense (UFF).

References

Alizadeh-Sania, M., Khezerloub, A., Ehsani, A., 2018. Fabrication and characterization of the bionanocomposite film based on whey protein biopolymer loaded with TiO2 nanoparticles, cellulose nanofibers and rosemary essential oil. Ind. Crop. Prod. 124, 300–315.

Candido, R.G., Godoy, G.G., Gonçalves, A.R., 2017. Characterization and application of cellulose acetate synthesized from sugarcane bagasse. Carbohydr. Polym. 167, 280–289.

Canevarolo Jr., S.V., 2006. Ciência dos Polimeros: Um texto básico para tecnólogos e engenheiros. Editora Artliber, São Paulo, pp. 17–19.

Castañón-Rodríguez, J.F., Torrestiana-Sánchez, B., Montero-Lagunes, M., Portilla-Arias, J., de León, J.R., Aguilar-Uscanga, M.G., 2013. Using high pressure processing (HPP) to pretreat sugarcane bagasse. Carbohydr. Polym. 98, 1018–1024.

Cerqueira, D.A., Filho, G.R., Carvalho, R.D.A., Valente, A.J.M., 2010. Caracterização de acetato de celulose obtido a partir do bagaço de cana-de-açúcar por 1H-RMN. Polímeros - Ciência Tecnol. 20, 85–91.

Chen, J., Xu, J., Wang, K., Cao, X., Sun, R., 2016. Cellulose acetate fibers prepared from different raw materials with rapid synthesis method. Carbohydr. Polym. 137, 685–692.

Cho, S., Lee, Y.S., Rhee, C., 2010. Edible oxygen barrier bilayer film pouches from corn zein and soy protein isolate for olive oil packaging. Food Sci. Technol. 43, 1234–1239.

Dannenberg, G.D.S., Funck, G.D., Cruxen, C.E.D.S., Marques, J.D.L., Silva, W.P.D., Fiorentini, Â.M., 2017. Essential oil from pink pepper as an antimicrobial component in cellulose acetate film: potential for application as active packaging for sliced cheese. LWT - Food Sci. Technol. 81, 314–318.

Fellows, P., 2006. Tecnologia do Processamento de Alimentos: princípios e prática, 2 ed. Artmed, Porto Alegre, p. 602.

Fraldi, M., Cutolo, A., Esposito, L., Perrella, G., Pastore Carbone, M.G., Sansone, L., Scherillo, G., Mensitieri, G., 2014. Delamination onset and design criteria of multilayer flexible packaging under high pressure treatments. Innovat. Food Sci. Emerg. Technol. 23, 39–53.

de Freitas, R.R.M., Senna, A.M., Botaro, V.R., 2017. Influence of degree of substitution on thermal dynamic mechanical and physicochemical properties of cellulose acetate. Ind. Crop. Prod. 109, 452–458.

Galazka, V.B., Dickinson, E., Ledward, D.A., 2000. Influence of high pressure processing on protein solutions and emulsions. Curr. Opin. Colloid Interface Sci. 5, 182–187.

Gonçalves, S.M., Santos, D.C., Motta, J.F.G., Ribeiro-Santos, R., Chávez, D.W.H., Melo, N.R., 2019. Structure and functional properties of cellulose acetate films incorporated with glycerol. Carbohydr. Polym. 209, 190–197.

Gross, M., Jaenicke, R., 1994. Proteins under pressure: the influence of high hydrostatic pressure on structure, function and assembly of proteins and protein complexes. Eur. J. Biochem. 221, 617–630.

Hasa, E., Stansbury, J.W., Guymon, C.A., 2020. Manipulation of crosslinking in photo-induced phase separated polymers to control morphology and thermo-mechanical properties. Polymer 122699.

Hernandez-Lzquierdo, V.M., Krochta, J.M., 2009. Thermal transitions and heat-sealing of glycerol-plasticized whey protein films. Packag. Technol. Sci. 22, 255–260.

Kendouli, S., khalfallah, O., Sobti, N., Bensouissi, A., Avci, A., Eskizeybek, V., Achour, S., 2014. Modification of cellulose acetate nanofibers with PVP/Ag addition. Mater. Sci. Semicond. Process. 428, 13–19.

Khaneghah, A.M., Hashemi, S.M.B., Limbo, S., 2018. Antimicrobial agents and packaging systems in antimicrobial active food packaging: an overview of approaches and interactions. Food Bioprod. Process. III, 1–19.

Liu, L., Gong, D., Bratasz, L., Zhu, Z., Wang, C., 2019. Degradation markers and plasticizer loss of cellulose acetate films during ageing. Polym. Degrad. Stabil. 168, 108952.

Marangoni Júnior, L., Marcelo, C., Marisa, P., Anjos, C.A.R., 2019. Effect of high-pressure processing on characteristics of flexible packaging for foods and beverages. Food Res. Int. 119, 920–930.

Marangoni Júnior, L., de Oliveira, L.M., Bócoli, P.F.J., Cristianini, M., Padula, M., Anjos, C.A.R., 2020a. Morphological, thermal and mechanical properties of polyamide and ethylene vinyl alcohol copolymer multilayer flexible packaging after high-pressure processing. J. Food Eng. 109913.

Marangoni Júnior, L., de Oliveira, L.M., Dantas, F.B.H., Cristianini, M., Padula, M., Anjos, C.A.R., 2020b. Influence of high-pressure processing on morphological, thermal and mechanical properties of retort and metallized flexible packaging. J. Food Eng. 273, 109812.

Martins, C.F., 2014. Tese. Efeito da tecnologia de alta pressão hidrostática nas características microbiológicas e físicas da tripa natural de suíno, 88. Universidade de Lisboa. Faculdade de Medicina Veterinária.

Melo, N.R., 2003. Avaliação de embalagem ativa por incorporação de nisina na inibição de *Stahylococcus* sp. Dissertação (Mestrado em Ciência e Tecnologia de Alimentos). -Universidade Federal de Viçosa, Viçosa, p. 73.

Mensitieri, G., Scherillo, G., Iannace, S., 2013. Flexible packaging structures for high pressure treatments. Innovat. Food Sci. Emerg. Technol. 17, 12–21.

Miles, D.C., Briston, J.H., 1975. Tecnologia Dos Polímeros, Poligono/Ed., p. 557 São Paulo.

Molinaro, S., Cruz-Romero, M., Sensidoni, A., Morris, M., Lagazio, C., Kerry, J.P., 2015. Combination of high-pressure treatment, mild heating and holding time effects as a means of improving the barrier properties of gelatin-based packaging films using response surface modeling. Innovat. Food Sci. Emerg. Technol. 30, 15–23.

Nascimento, T.A., Calado, V., Carvalho, C.W.P., 2012. Development and characterization of flexible film based on starch and passion fruit mesocarp flour with nanoparticles. Food Res. Int. 49, 588–595.

Oliveira, T.L.C.D., Ramos, A.L.S., Ramos, E.M., Piccoli, R.H., Cristianini, M., 2015. Natural antimicrobials as additional hurdles to preservation of foods by high pressure processing. Trends Food Sci. Technol. 45, 60–85.

Rana, D., Cho, K., Woo, T., Lee, B.H., Choe, S., 1999. Blends of ethylene 1-octene copolymer synthesized by Ziegler–Natta and metallocene catalysts. I. Thermal and mechanical properties. J. Appl. Polym. Sci. 74, 1169–1177.

Rana, D., Kim, H.L., Kwag, H., Rhee, J., Cho, K., Woo, T., Choe, S., 2000. Blends of ethylene 1-octene copolymer synthesized by Ziegler–Natta and metallocene catalysts. II. Rheology and morphological behaviors. J. Appl. Polym. Sci. 76, 1950–1964.

Richardson, E., Giachet, M.T., Schilling, M., Learner, T., 2014. Assessing the physical stability of archival cellulose acetate films by monitoring plasticizer loss. Polym. Degrad. Stabil. 107, 231–236.

Romani, V.P., Prentice-Hernández, C., Martins, V.G., 2017. Active and sustainable materials from rice starch, fish protein and oregano essential oil for food packaging. Ind. Crop. Prod. 97, 268–274.

Sarafraz, M.M., Arjomandi, M., 2019. Contact angle and heat transfer characteristics of a gravity-driven film flow of a particulate liquid metal on smooth and rough surfaces. Appl. Therm. Eng. 149, 602–612.

Siracusa, V., Rocculi, P., Romani, S., Rosa, M.D., 2008. Biodegradable polymers for food packaging: a review. Trends Food Sci. Technol. 19, 634–643.

Song, X., Zhang, K., Song, Y., Duan, Z., Liu, Q., Liu, Y., 2020. Morphology, microstructure and mechanical properties of electrospun alumina nanofibers prepared using different polymer templates: a comparative study. J. Alloys Compd. 154502.

Stratakos, A.C., Delgado-Pando, G., Linton, M., Patterson, M.F., Koidis, A., 2015. Synergism between high-pressure processing and active packaging against *Listeria monocytogenes* in ready-to-eat chicken breast. Innovat. Food Sci. Emerg. Technol. 27, 41–47.

Teles, A.S.C., Chávez, D.W.H., Oliveira, R.A., Bon, E.P.S., 2019. Use of grape pomace for the production of hydrolytic enzymes by solid-state fermentation and recovery of its bioactive compounds. Food Res. Int. 120, 441–448.

Wan Daud, W.R., Djuned, F.M., 2015. Cellulose acetate from oil palm empty fruit bunch via a one step heterogeneous acetylation. Carbohydr. Polym. 132, 252–260.

Yoo, S., Holloman, C., Tomasko, D., Koelling, K., Pascall1, M.A., 2013. Effect of high pressure processing on the thermal and mechanical properties of polyethylene films measured by dynamical mechanical and tensile analyses. Packag. Technol. Sci. 27, 169–178.

Zizovic, I., Senerovic, L., Moric, I., Adamovic, T., Jovanovic, M., Krusic, M.K., Milovanovic, S., 2018. Utilization of supercritical carbon dioxide in fabrication of cellulose acetate films with anti-biofilm effects against *Pseudomonas aeruginosa* and *Staphylococcus aureus*. J. Supercrit. Fluids 140, 11–20.